Progress In Electromagnetics Research C, Vol. 129, 245–256, 2023

High-Power Ka-Band Extended Interaction Klystron Design Based on Internal Coupling Cavity

Bingchuan Xie[1, 2], Rui Zhang[1, *], Yong Wang[1, 2], Xu Zhang[1, 2], Xiudong Yang[1], Yunfeng Liao[1], and Zhihui Geng[1]

Abstract—A high-efficiency interaction circuit for Ka-band klystron has been proposed based on a novel internal coupling cavity. Driven by a 25 kV, 5 A pencil beam, the interaction circuit can produce a peak output power of 38.4 kW at Ka-band, and the electronic efficiency is 30.7%. The electromagnetic properties of the unequal slot multi-gap cavity and internal coupling cavity have been studied and compared. The internal coupling cavity demonstrated a higher coupling coefficient and characteristic impedance than the unequal slot multi-gap cavity, which can improve the circuit efficiency. Stability and pattern analysis have been performed on the output cavity. A four-gap output cavity has been designed. Simulation results show that there is no mode competition and oscillation in the output cavity. The corresponding beam optics has also been designed to produce the required beam. Compared with the existing work, the interaction circuit can produce almost twice the output power with the same beam voltage and Brillouin focusing magnetic field. The efficiency is also improved by 6 percent.

1. INTRODUCTION

High-power millimeter sources play a critical part in detection, communication and imaging. Vacuum electronic devices such as traveling wave tubes, klystrons, and gyrotrons can generate the required high-power microwave. The extended interaction klystron exhibits high power potential in MMW and THz frequency bands [1, 2]. The multi-gap resonator used in the extended klystron can provide a large characteristic impedance, which can overcome the disadvantage of the traditional single-gap resonator encountered in high frequency bands [3]. Higher characteristic impedance means a shorter interaction circuit, which can bring advantages in beam optics design. In the output section of the klystron, a multi-gap output cavity with a larger equivalent characteristic impedance can significantly improve the bandwidth and efficiency of the klystron [4].

The extended interaction klystron based on multi-gap cavities has shown great power potential in recent years. CPI (Communications & Power Industries Canada Inc) announced in 2007 that it had developed a series of state-of-the-art extended interaction klystrons for deep space exploration, radar, and imaging. The designed high-power klystron can generate a high peak output power of 1000 W and a bandwidth of 300 MHz. Furthermore, Zhao et al. built a Ka-band klystron that can produce a peak output power of 20.3 kW [5]. The electron beam used to drive that klystron was a 27 kV and 3 A pencil beam. Moreover, Chen et al. built a high peak power klystron that can produce a peak power of 930 W in the Ka-band [6]. To drive the X-ray free electron laser (FEL) in European, a 2 MW Ka-band klystron has been designed [7]. The 2 MW Ka-band klystron has twenty 60 kV, 6 A pencil beams

Received 10 November 2022, Accepted 11 January 2023, Scheduled 9 February 2023

* Corresponding author: Rui Zhang (ruizhang@mail.ie.ac.cn).

[1] Key Laboratory of Science and Technology on High Power Microwave Sources and Technologies, Aerospace Information Research Institute, Chinese Academy of Sciences, Beijing 100190, China. [2] School of Electronic, Electrical and Communication Engineering, University of Chinese Academy of Sciences, Beijing 100049, China.

Furthermore, sheet beam extended interaction klystron can produce multi-kilowatt peak power in W-band. The Naval Research Laboratory (NRL) has reported a sheet beam klystron that can generate an output power of 7.7 kW in W-band [8]. The University of California, Davis (UC Davis) has also reported a sheet beam extended klystron that can generate a peak output power of 56 kW [9], and the corresponding efficiency is 20 percent.

Although the multi-gap cavity has a large characteristic impedance, more axial modes have also been introduced. N gaps cavity has N axial modes [10]. Those axial modes increase the possibility of mode competition and oscillation in extended interaction klystron. Some new variations of the multi-gap cavity have been proposed. In high-frequency bands, higher characteristic impedance is desirable for better performance. The narrow coupling cavity can increase the characteristic impedance by putting more energy in the central gaps of the cavity [2, 11]. Xie et al. have proposed a novel type of coupling cavity called internal coupling cavity which can further increase the characteristic impedance [12]. Moreover, the unequal-slot multi-gap cavity has been proposed to increase the axial mode separation and the klystron bandwidth [13, 14]. However, the axial field distribution of the unequal-slot multi-gap cavity is unequal, which decreases the characteristic impedance and the klystron efficiency.

In order to further improve the output power and efficiency of the Ka-band klystron, we have designed an extended interaction klystron based on an internal coupling cavity with a larger drift tube and higher beam current. The operating voltage is fixed at 25 kV to maintain a compact high voltage power supply. The total beam current is 5 A so that such a beam can be focused by a uniform magnetic field about 0.6 T. Such beam voltage and current make the whole klystron lighter and more compact for high-power radar applications. Moreover, a detailed study has been performed on the unequal-slot multi-gap cavity and internal coupling cavity. Furthermore, Xie et al. did not use the coupling cavity in the whole interaction circuit but only used this cavity as the output cavity. Because the coupling coefficient of single-gap resonance is smaller than that of multi-gap cavities operating in π mode, the interaction efficiency is reduced. To explore the power potential of this internal coupling cavity, we have designed a Ka-band extended interaction klystron with high peak power based on this novel internally coupled resonator. It can produce an output power of 37.8 kW in the Ka-band and an efficiency of 30.7%. The beam optics are also presented in this paper.

2. PARAMETER DESIGN OF THE KLYSTRON

The designed beam voltage is 25 kV, and the beam current is 5 A. The beam radius is 0.45 mm, and the drift tube radius is 0.65 mm with a filling factor of 0.69. The Brillouin magnetic field used to focus the electron beam is given by $B_b = 0.83 \times 10^{-3}(I_0)^{1/2}/(R_b {V_0}^{1/4})$, which is 0.33 T. The whole parameters are summarized in Table 1.

Table 1. Design parameters of the Ka-band klystron.

Parameters	Values	Unit
beam voltage	25	kV
beam current	5	A
perveance	1.27	μp
beam radius	0.45	mm
drift tube radius	0.65	mm
Brillouin magnetic field (B_b)	0.33	T

3. INTERNAL COUPLING CAVITY ANALYSIS AND DESIGN

3.1. Comparison of Electromagnetic Characteristics of Two Cavities

To study the electromagnetic characteristics of this kind of internal coupling cavity, we selected the unequal-slot resonators in [5] for comparison. The lengths of the long slot and short slot are almost

the same (4.71 mm and 4.03 mm in [5] and ours for 4.74 mm and 0.395 mm). The electromagnetic characteristics of a resonator are usually characterized by two parameters: characteristic impedance R/Q and coupling coefficient M. Higher characteristic impedance means stronger beam-wave interaction. The coupling coefficient has a crucial effect on efficiency. The reason that the efficiency of the klystron decreases at high-frequency bands is the decrease in the coupling coefficient of the resonator. The characteristic impedance R/Q and coupling coefficient M are given by (1) and (2), respectively [15], where E_z is the axial field distribution, $\omega = 2\pi f$ the angular frequency of the mode, W_s the total energy stored in the resonator (set as 1 W in CST), and β the propagation constant of the electron beam.

$$R/Q = \frac{\left(\int_{-\infty}^{\infty} |E_z|\, dz\right)^2}{(2\omega W_s)} \tag{1}$$

$$M = \frac{\int_{\infty}^{\infty} E_z e^{j\beta z} dz}{\int_{\infty}^{\infty} |E_z|\, dz} \tag{2}$$

Figure 1 shows a schematic diagram of the designed three-gap internal coupling resonator. The coupling coefficient and characteristic impedance play a critical role in determining the efficiency, output power, and bandwidth of klystron. p is the period of the gaps, which is the distance between two adjacent gaps. g is the gap width; sw and sh are the width and height of the coupling cavity; and cw is the width and height of the central gaps. A square cavity has been chosen to ensure the uniformity of the field in the circumferential direction. The coupling coefficient of the resonator plays an important role in the efficiency of the interaction circuit. The π mode has the highest coupling coefficient among the multiple axial modes of a resonator. Here, we choose π mode as the working mode. The period p is an important matching parameter that features the synchronization of the electron beam and electromagnetic wave. p is given by (3), where N is 1; ve is the electron velocity; and f_0 is the operating frequency. The size parameters of the two resonators are given in Table 2.

$$p = \frac{N v_e}{f_0} \tag{3}$$

The electric field distributions of the two resonators are given by the electromagnetic simulation software CST. Fig. 2 shows the axial electric field distribution of the two resonators. The electric field of the internal coupling cavity in the middle gap is stronger than the unequal-slot cavity due to the smaller volume of the internal coupling cavity. Novel cavity has a smaller equivalent capacitance C from the equivalent circuit point of view, while $R/Q = \sqrt{L/C}$, and hence its characteristic impedance

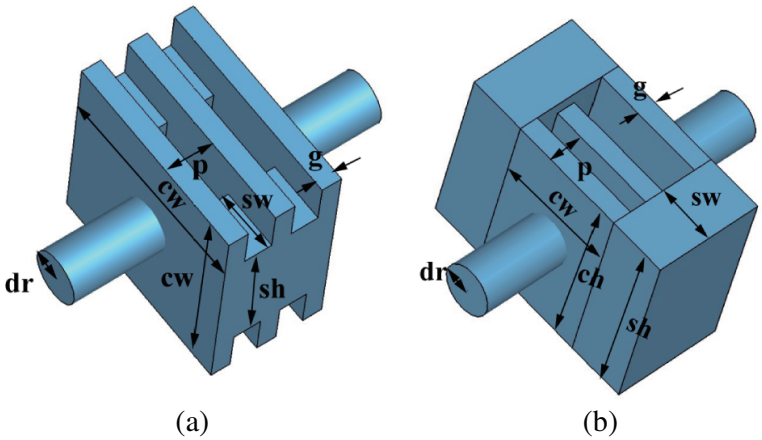

Figure 1. Novel internal coupling three-gap cavity (a) and unequal-slot multi-gap cavity (b).

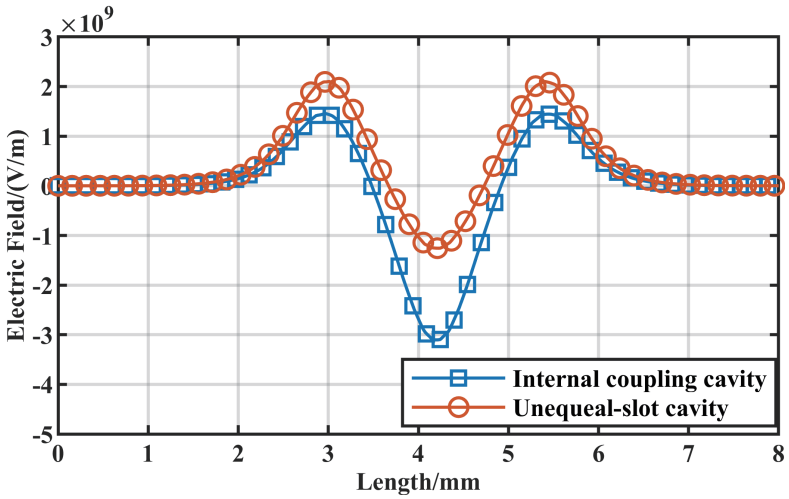

Figure 2. Field distribution along axial direction of the internal coupling cavity and unequal-slot cavity.

Table 2. Parameters of the designed two three-gap cavities.

Parameters	Internal coupling cavity (mm)	Unequal-slot cavity (mm)
dr	0.65	0.65
cw	5.11	3
ch	5.11	4.74
p	1.2	1.2
sh	3	4.74
sw	1.5	1.5
g	0.5	0.5

Table 3. High-frequency characteristic parameters comparison between internal coupling cavity and the unequal-slot cavity.

	Internal coupling cavity	Unequal-slot cavity
gaps	3	3
frequency/GHz	35.01	35.00
$R/Q/\Omega$	58.3	52
M	0.7238	0.6850
$M^2R/Q/\Omega$	30.71	24.60

is larger. Table 3 shows the specific comparison of electromagnetic properties. It can be seen from the table that the internal coupling multi-gap cavity has a higher coupling coefficient and characteristic impedance than the unequal-slot cavity.

3.2. Stability Analysis

The multi-gap output cavity will introduce more axial modes, which may lead to mode competition in the output cavity. In this section, we perform mode stability analysis on different multi-gap resonators. A four-gap coupling cavity has been determined to be used in high frequency circuit. The mode separation

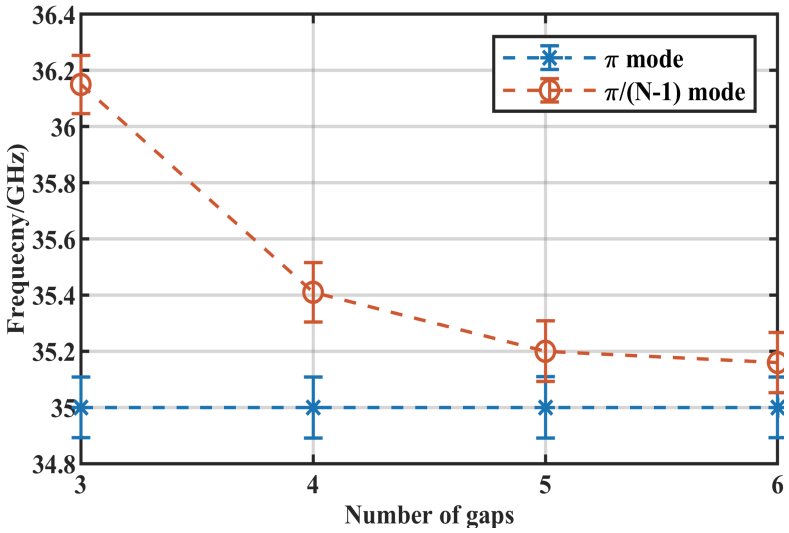

Figure 3. Mode separation between of the π mode and the $\pi(N-1)/N$ mode versus number of gaps.

of the operating mode and the adjacent axial mode is shown in Fig. 3. The height of the error bar is equal to the 3-dB bandwidth (Δf) of the corresponding mode, which is equal to $\Delta f = f_L/Q_L$, where $Q_L = Q_e Q_0/(Q_e + Q_0)$ [15]. Here, we assume that Q_e is 1/4 Q_0. As can be seen from Fig. 3, when the number of gaps reaches four, the two adjacent modes begin to overlap. Therefore, the maximum of four gaps can be used in the output cavity.

In addition, the dispersion curve of the multi-gap resonator can characterize the synchronization characteristics of the electron beam and the electromagnetic wave, which can be used to investigate the possible competitive mode. Fig. 4 shows the dispersion curve of the four-gap output cavity and the electron beam curve at 25 kV. As can be seen from Fig. 4, the π mode is closest to the beam line, and the other modes do not intersect it. Therefore, other axial modes will not synchronize with the beam; the π mode can work stably. The equivalent characteristic impedance (M^2R/Q)) of each mode also reflects the beam-wave interaction ability of that mode. Fig. 5 shows the high-frequency properties of the different axial modes of the four-gap output cavity. Although other axial modes have larger R/Q, the coupling coefficient M is smaller than the operating mode. Therefore, they will not be strong competitive modes.

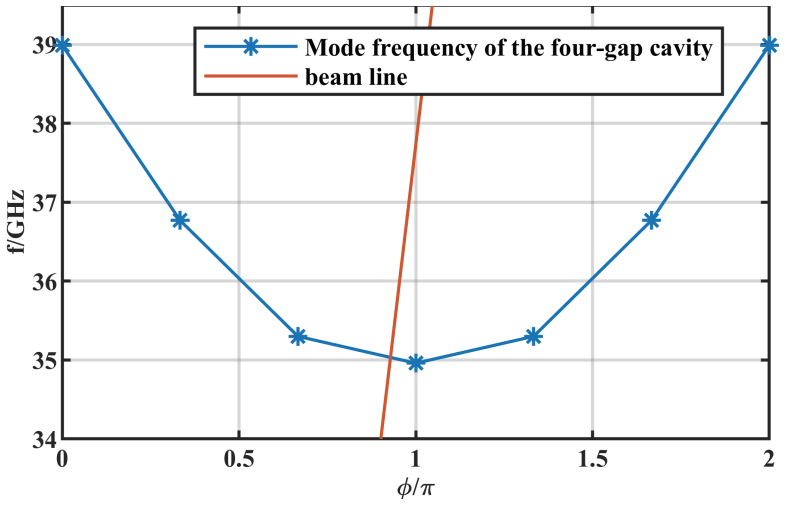

Figure 4. Dispersion curve and the beam line of the four-gap output cavity.

	π mode	1/3 π mode	2/3 π mode	2π mode
Patterns of the electric field	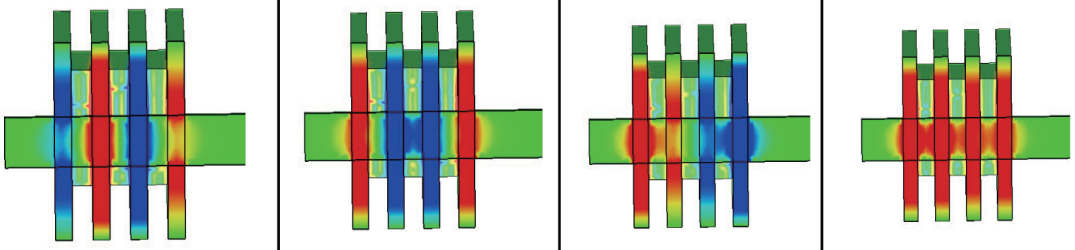			
mode frequency	34.96 GHz	35.30 GHz	36.77 GHz	38.99 GHz
M	0.77	0.30	0.15	0.12
R/Q	55.5 Ω	90.4 Ω	106.7 Ω	133.0 Ω
M^2R/Q	32.5 Ω	8.4 Ω	2.4 Ω	2.1 Ω

Figure 5. High frequency properties of the different axial modes.

Drift tube radius is a key factor when a klystron is designed. A smaller drift tube radius means higher M and high klystron efficiency. However, a smaller drift tube will decrease the total beam current under the same focusing magnetic field, which means that the klystron can carry less DC power. Fig. 6 shows the M vs drift tube radius. As the drift tube becomes smaller, the coupling coefficient and focusing magnetic field increase. The drift tube radius was fixed at 0.65 mm to maintain a relatively high M and low focusing magnetic field. The variation is based on the same filling factor and beam voltage.

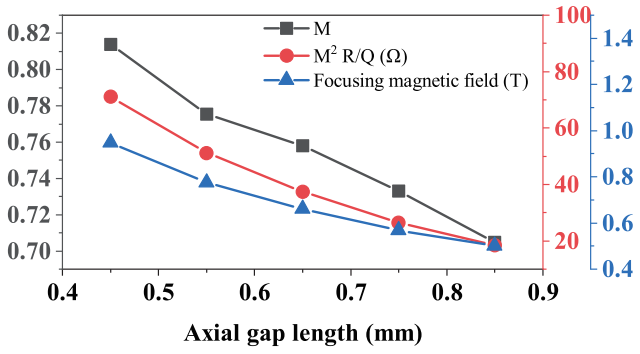

Figure 6. M, M^2R/Q, and focusing magnetic field vs axial gap length.

3.3. Sensitivity Analysis of the Output Cavity

In millimeter wave band, the size of the resonator becomes very small. Therefore, it is necessary to get the size sensitivity of the resonator. The dimensional accuracy of computerized numerical control

(CNC), high precision machining is ±5 µm. The size deviation will affect the resonant frequency of the resonator. The frequency of the resonator has an important effect on the efficiency of the interaction circuit. Therefore, it is necessary to explore the impact of manufacturing errors on the frequency of the internal coupling cavity. We selected a three-gap middle cavity as the research object and added a random machining error of ±5 µm to each of its dimensions. One hundred models with tolerance were built in CST, and then their frequencies were obtained by writing code. The obtained frequency distribution is shown in Fig. 7. In this polar plot, the R axis is the absolute value of the frequency change. The Phi axis is the argument of the complex number formed by the variation of the selected two dimensions. The selected two dimensions are *cw* and *sw*. For example, if the size of *cw* is changed by 2 µm, and the size of *sw* is changed by 2 µm, then the argument formed is 45°. The statistical results show that 63% of the frequency changes are less than 20 MHz. Almost all frequency deviations of models are less than 40 MHz, which is tolerable in consideration of the klystron bandwidth.

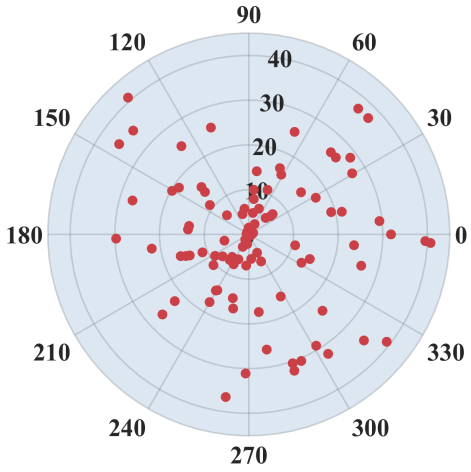

Figure 7. Frequency deviation distribution of the model with tolerance.

3.4. Interaction Circuit Design

An interaction circuit consisting of four multi-gap resonators has been designed. The 3D simulation model established in CST Particle Studio is shown in Fig. 8. One three-gap input cavity, two three-gap middle cavities, and one four-gap output cavity are used. The input cavity and middle cavity are both three-gap resonators, which can avoid the mode competition caused by the axial modes to the maximum extent. Using more gaps in the output cavity can improve the ability to extract energy from the bunched electron beam. Multiple gaps mean greater characteristic impedance, which can shorten the length of the interaction circuit and reduce the focusing pressure of the beam optics. The length

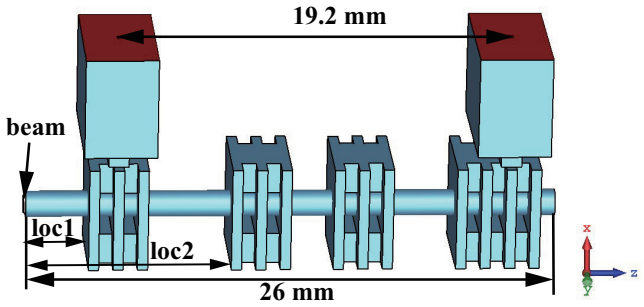

Figure 8. Diagram of the whole interaction circuit.

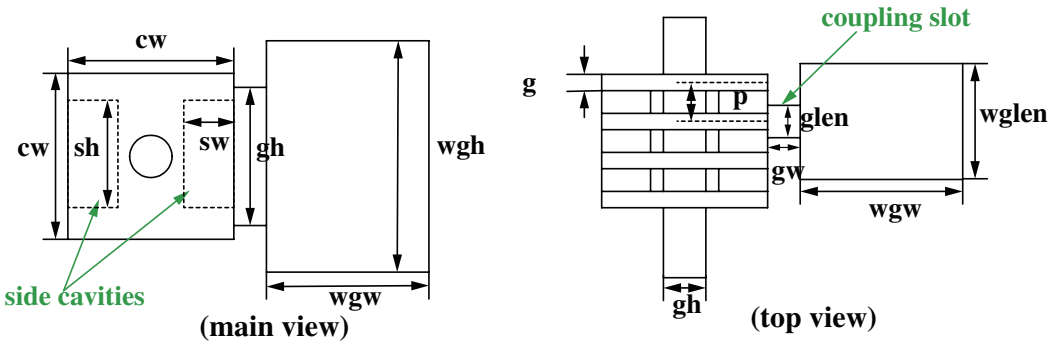

Figure 9. Diagram of the whole interaction circuit.

of the entire interaction circuit is only 26 mm. This is due to the high characteristic impedance and coupling coefficient of the internal coupling multi-gap resonator. Schematic view of the four-gap output cavity is shown in Fig. 9. The input and output cavities adopt WR-28 (7.11 mm × 3.56 mm) waveguide for energy input and output. The waveguide side extension wgw is 5 mm. The structure of the input cavity is very similar to the output cavity, except for the location of coupling slot. The coupling slot of the input cavity is located at the central gap, while the coupling slot of the output cavity is aligned with the penultimate gap. Side cavities in all multi-gap cavities share the same dimensions ($sh = 3$ mm, $sw = 1.5$ mm). The central gaps of all multi-gap cavities are square. Parameter of cw is varied to adjust the resonant frequency of each multi-gap cavity. To alleviate the fabrication pressure, the period and axial length of gaps are kept the same for four cavities ($p = 1.2$ mm, $g = 0.5$ mm). The position of each cavity is calculated from its leftmost face (as shown in Fig. 8). Coupling slots of the input cavity and output cavity are optimized to obtain the highest output power. The coupling slots have the same axial length and side extension ($glen1 = glen4 = 1$ mm, $gw1 = gw4 = 1$ mm) but different slot heights ($gh1 = 3.9$ mm, $gh4 = 4.25$ mm).

The specific parameters of cavities used in the designed extended interaction circuit are summarized in Table 4. The designed interaction circuit can achieve 38.4 kW output power with a 245 mW energy input. Fig. 10 shows the output signal of the output port recorded in the CST simulation. The output signal reaches stability after about 15 ns and can be stable without oscillation for 100 ns. The Fourier transform of the output signal is also shown in Fig. 10. The signal spectrum is very clean, and there is no mode contention. Fig. 11 shows the phase space diagram of the particle and the frequency sweep curve. The particles, after modulation, can greatly slowdown in the output cavity to give up energy to the electromagnetic wave. The normalized E_z distribution (the dotted line in Fig. 11) also indicates

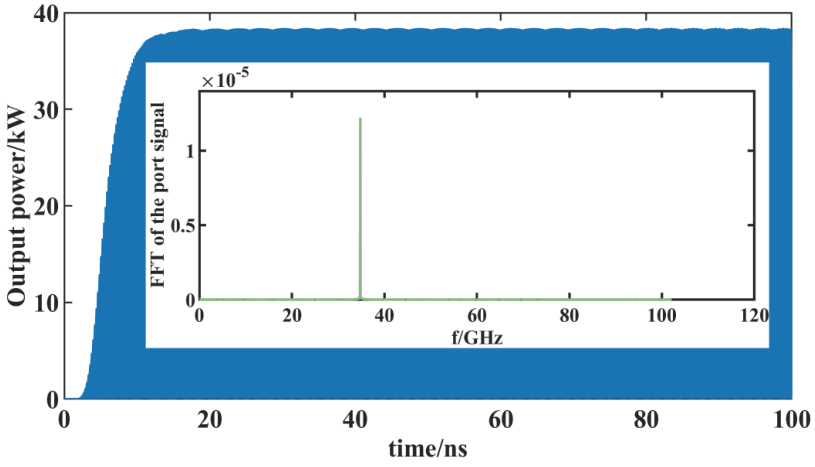

Figure 10. Output signal and its Fourier spectrum.

Table 4. Parameters of cavities used in the designed extended interaction circuit.

N	f (GHz)	R/Q (Ω)	M	Qe	$M^2(R/Q)$ (Ω)	cw (mm)	location (mm)
1	34.93	47.8	0.72	960	24.8	5.13	3
2	34.89	57.5	0.73	1290	30.6	5.13	10
3	35.00	57.7	0.73	1290	30.7	5.11	15
4	34.96	55.5	0.77	600	32.9	5.10	21

that the electric field excited by the modulated beam becomes stronger as electrons travel longer along Z axis. The energy of some electrons can be slowed down to below 5 keV. The equal excitation 3 dB bandwidth of the interaction circuit is 140 MHz. Fig. 12 shows the klystron output power with different input powers. Output power reaches saturation when input power is about 0.25 W. In this case, the gain is 51.9 dB.

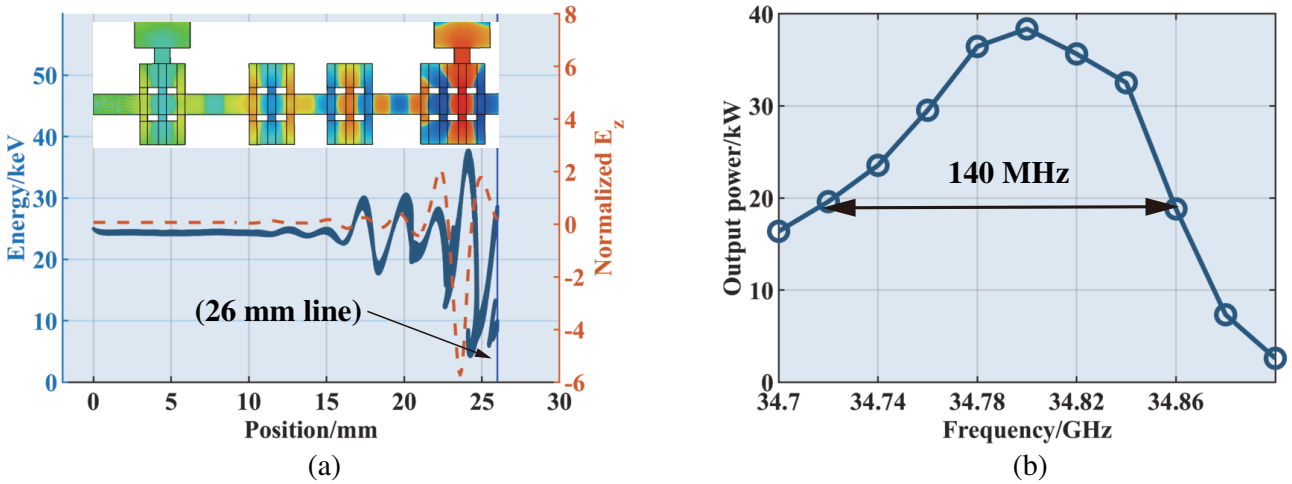

Figure 11. Particle phase space diagram (a) and frequency sweep curve (b).

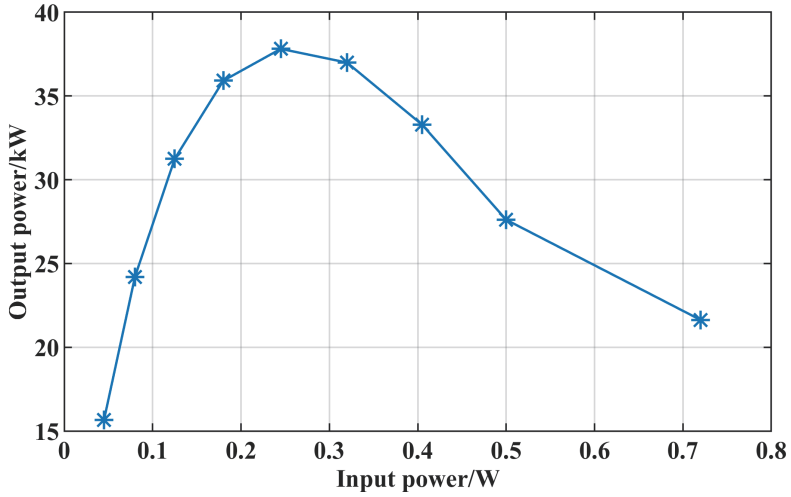

Figure 12. Output power versus input power.

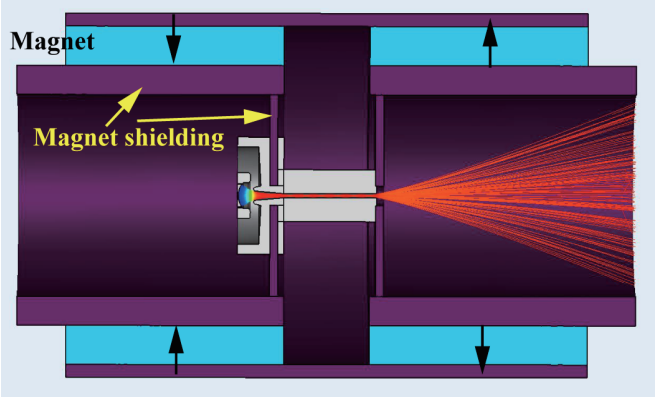

Figure 13. Diagram of the designed beam optics system.

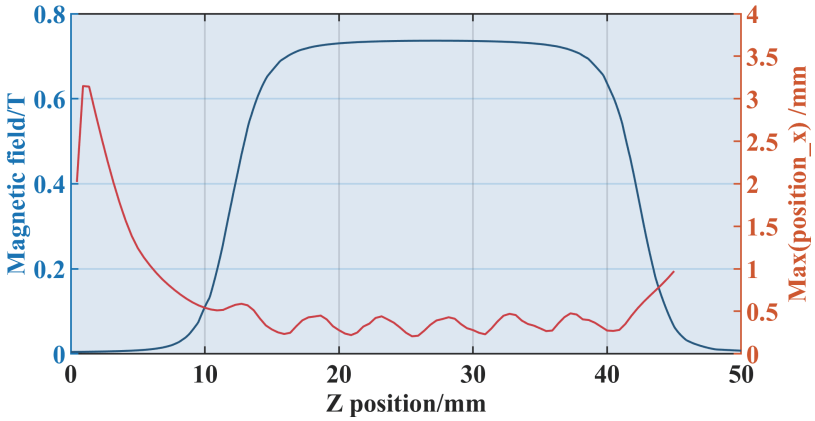

Figure 14. Axial magnetic field distribution in beam optics and beam envelops.

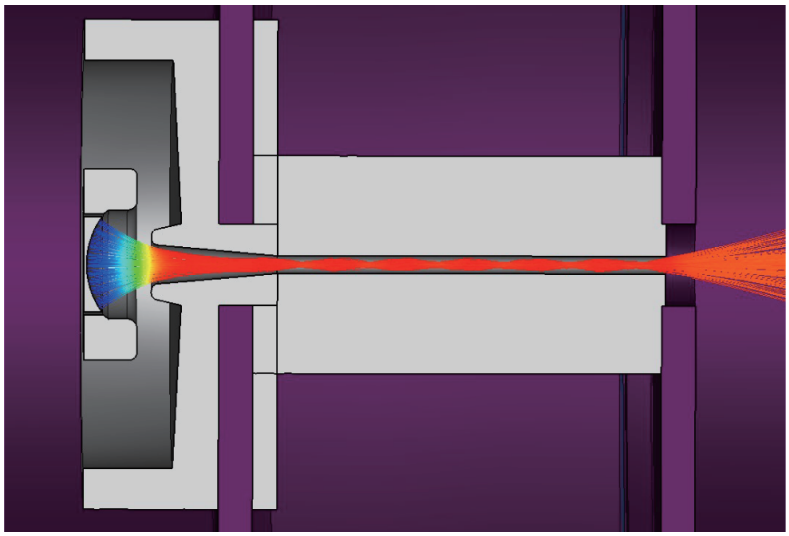

Figure 15. Trajectories of electrons.

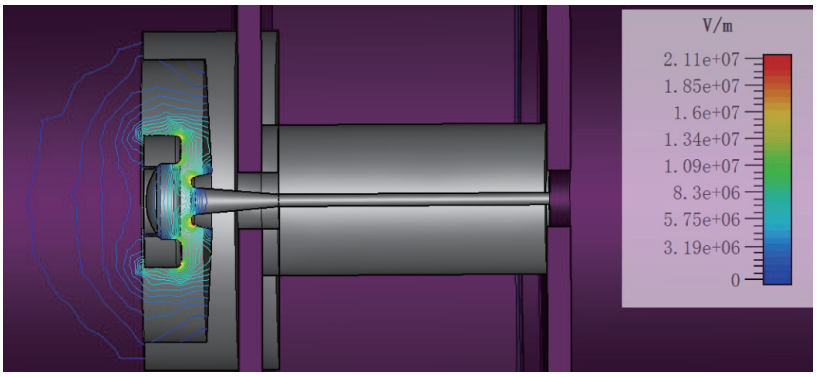

Figure 16. Electric field distribution in the gun area.

4. BEAM OPTICS DESIGN

A matching beam optics has been designed. The 25 kV, 5 A pencil beam is focused by the uniform magnetic field produced by two symmetrical ring magnets. Such a magnet structure is simple, robust, and suitable for short distance electron beam focusing. The structure diagram of the designed beam optics system is shown in Fig. 13. Fig. 14 shows the envelope of the electron beam and the distribution of the axial magnetic field. The waist radius of the beam reaches the required 0.45 mm. The focusing magnetic field produced by the permanent magnet is 0.73 T. In the simulation, 99% of the electrons can pass through the drift tube. Fig. 15 shows the details of the electron trajectory. Fig. 16 shows the distribution of the electric field in the electron gun region. CST simulation results show that the maximum electric field strength is 21 MV/m, which is well below the limiting value of 30 MV/m. By optimizing the beam optics dimensions, a 25 kV and 5 A pencil beam is obtained.

5. CONCLUSIONS

In this paper, an extended interacting klystron operating at Ka-band is designed based on the internal coupling multi-gap resonators. With such high coupling coefficient resonators, a high efficiency of 30.7% is obtained. The klystron is able to generate a peak power of 38.4 kW with a 26 mm long interaction circuit. Compared with Ref. [5], the Ka-band klystron demonstrated in this paper has almost twice the output power and a 6 percent improvement in efficiency, and the interaction circuit is shorter. The operating voltage and Brillouin magnetic field used to focus the pencil beam are the same. The high-frequency characteristic parameters of the internal coupling cavity and the unequal-slot multi-gap resonator are compared and analyzed. The internal coupling cavity shows a larger coupling coefficient and characteristic impedance than the traditional unequal-slot cavity. Multi-gap cavity modes stability analysis ensures the stability of the interaction circuit. Particle in cell (PIC) simulation results demonstrate the advantages of internal coupling resonators in improving efficiency. The corresponding electron optical system is designed, and the electron beam can be transmitted stably in a drift tube with small fluctuations.

ACKNOWLEDGMENT

This work was supported by the Scientific Instrument Developing Project of the Chinese Academy of Sciences (YJKYYQ20180005) and National MCF Energy R&D Program (2018YFE0305100).

REFERENCES

1. Xu, X., X. Yuan, H. Li, et al., "Design of a G-band extended interaction klystron based on a three-coupling-hole structure," *IEEE Trans. Electron Devices*, Vol. 69, No. 3, 1368–1373, 2022, doi: 10.1109/ted.2021.3138840.
2. Guo, N., Q. Xue, Z. Qu, et al., "Study of a 0.34-THz ladder-type extended interaction klystron with narrow coupling cavities," *IEEE Trans. Electron Devices*, Vol. 68, No. 11, 5851–5857, 2021, doi: 10.1109/TED.2021.3114392.
3. Chodorow, M. and T. Wessel-Berg, "A high-efficiency klystron with distributed interaction," *IRE Transactions on Electron Devices*, Vol. 8, No. 1, 44–55, 1961.
4. Yaogen, D., *Design, Manufacure and Application of High Power Klystron*, National Defense Industry Press, Beijing, 2010.
5. Zhao, D., W. Gu, X. Hou, G. Liu, Q. Xue, and Z. Zhang, "Demonstration of a high-power Ka-band extended interaction klystron," *IEEE Trans. Electron Devices*, Vol. 67, No. 9, 3788–3794, 2020, doi: 10.1109/TED.2020.3008881.
6. Wei Yuan, C. and C. Kwo Ray, "A high-duty Ka-band extended interaction klystron," *2008 IEEE International Vacuum Electronics Conference*, 201–202, April 22–24, 2008, doi: 10.1109/IVELEC.2008.4556337.
7. Cai, J. C., I. Syratchev, and G. Burt, "Design study of a high-power Ka-band high-order-mode multibeam klystron," *IEEE Trans. Electron Devices*, Vol. 67, No. 12, 1–7, 2020, doi: 10.1109/TED.2020.3028348.
8. John Pasour, E. W., K. T. Nguyen, A. Balkcum, F. N. Wood, R. E. Myers, and F. Baruch Levush, "Demonstration of a multikilowatt, solenoidally focused sheet beam amplifier at 94 GHz," *IEEE Trans. Electron Devices*, Vol. 61, No. 6, 1630–1636, 2014, doi: 10.1109/TED.2013.2295771.
9. Gamzina, D., L. R. Barnett, B. Ravani, and N. C. Luhmann, "Mechanical design and manufacturing of W-band sheet beam klystron," *IEEE Trans. Electron Devices*, Vol. PP, No. 99, 1–8, 2017, doi: 10.1109/TED.2017.2690642.
10. Fujisawa, K., "The Laddertron — A new millimeter wave power oscillator," *IEEE Trans. Electron Devices*, Vol. 11, No. 8, 381–391, 1964.
11. Li, S., C. Ruan, A. K. Fahad, P. Wang, Z. Zhang, and W. He, "Novel coupling cavities for improving the performance of G-band ladder-type multigap extended interaction klystrons," *IEEE Transactions on Plasma Science*, Vol. 48, No. 5, 1350–1356, 2020.
12. Xie, B., R. Zhang, Y. Wang, et al., "Design of a high-power V-band klystron with internal coupling multigap cavity," *IEEE Trans. Electron Devices*, Vol. 69, No. 5, 2644–2649, 2022, doi: 10.1109/TED.2022.3159260.
13. Li, R., C. Ruan, A. K. Fahad, C. Zhang, and S. Li, "Broadband and high-power terahertz radiation source based on extended interaction klystron," *Scientific Reports*, Vol. 9, No. 1, 2019.
14. Li, R., C. Ruan, and H. Zhang, "Design and optimization of G-band extended interaction klystron with high output power," *Physics of Plasmas*, Vol. 25, No. 3, 033107, 2018, doi: 10.1063/1.5012018.
15. Shin, Y. M., J. X. Wang, L. R. Barnett, and N. C. Luhmann, "Particle-in-cell simulation analysis of a multicavity W-band sheet beam klystron," *IEEE Trans. Electron Devices*, Vol. 58, No. 1, 251–258, 2010.